OPEN ACCESS
IOP Publishing
Journal of Optics
J. Opt. **26** (2024) 065502 (10pp)
https://doi.org/10.1088/2040-8986/ad3cf3

Circular dichroism in nonlinear topological Weyl semimetals

Helda Alomeare[1], Ferhat Nutku[2,*] and Mustafa Sarısaman[2]

[1] Institute of Graduate Studies in Science, İstanbul University, Vezneciler, İstanbul 34134, Turkey
[2] Department of Physics Faculty of Science, İstanbul University, Vezneciler, İstanbul 34134, Turkey

E-mail: fnutku@istanbul.edu.tr

Received 27 December 2023, revised 22 March 2024
Accepted for publication 10 April 2024
Published 30 April 2024

Abstract

In recent years, the field of topological photonics has emerged as a promising area of research due to its potential for the development of new photonic devices with unique properties. Topological Weyl semimetals (TWSs), which are characterized by the presence of Weyl points in their electronic band structure, are one such example of a material with interesting topological properties. In this study, Kerr and Faraday rotations were used to determine the nonlinear characteristics of TWSs. We focused on surfaces where no Fermi arcs are involved, so that Maxwell's equations would contain some peculiar topological terms. In Weyl semimetals with a specific topology, the distance between Weyl nodes aligned along the z-direction functions as a magnet. This results in a significant polar Kerr/Faraday rotation effect that is proportional to the separation distance, when light is directed onto the surface of the TWS that lacks Fermi arc states. Conversely, when the light is directed onto a surface with Fermi arc states, the Voigt effect is quadratically proportional to the separation distance. We considered electromagnetic wave propagation in a nonlinear Kerr-type medium. We have derived and solved the linear and nonlinear Helmholtz equations for TWSs using the tanh method. Our findings reveal that wave solutions could have some potentially significant implications for the design and optimization of photonic devices based on TWSs.

Supplementary material for this article is available online

Keywords: nonlinear differential equation, Helmholtz equation, topological Weyl semimetals, Fermi arcs

1. Introduction

Topological Weyl semimetals (TWSs) have been the focus of attention in recent years because of their band structures and Fermi arcs on their surfaces. A Weyl semimetal is a type of material that exhibits interesting electronic properties due to the existence of Weyl nodes. Weyl nodes are the points in momentum space where states cross each other in the electronic band structure. These nodes are protected by certain symmetries and give rise to interesting phenomena, such as Fermi arcs on the surfaces of the material. Fermi arcs are surface states that connect the projected locations of the Weyl nodes on the material's surface. These Fermi arcs are protected by the topology of the material and are robust against certain perturbations, such as elastic, electronic, structural and chemical perturbations. In a TWS material, the topological properties are preserved in such a way that the corresponding Weyl nodes are not affected and Fermi arcs are present on its surfaces. The interactions of these materials with electromagnetic waves are very interesting and have the potential to lead important applications, particularly in the development of new

* Author to whom any correspondence should be addressed.

photonic devices. Once electromagnetic waves are incident on a TWS surface which does not contain a Fermi arc, the polarization directions of the reflected and transmitted waves change due to the Kerr and Faraday rotations. This leads to the modified Maxwell equations involving topological terms in the source parts [1–5]. We avoid using the transverse magnetic (TM) mode in our analysis because it is not possible to observe Kerr/Faraday rotations with the TM mode. TM mode configuration requires the formation of an induced current in the material. We did not focus on the TM mode, as this indicates that it is more remarkable to examine this situation separately. We reserve the discussion of TM mode configuration for another work.

Merging the modified Maxwell equations leads to the linear Helmholtz equation, which can be solved using common differential equation solving routines. On the other hand, considering a nonlinear dielectric constant in the modified Maxwell equations leads to a nonlinear Helmholtz equation, the solutions of which can be found using the tanh method [6, 7].

Besides having many attractive and distinguished fundamental interests, Weyl semimetals may also offer new opportunities in practical applications, such as the construction of topological lasers [8, 9] and coherent perfect absorber (CPA) devices, compact optical isolators and circulators, orbital angular momentum detectors, higher-order harmonic generation, and nonreciprocal thermal emitters. Using Weyl semimetals, an optically active topological laser system can be obtained by means of spectral singularities [10–16]. Using the topological properties of Weyl semimetals, a stable excellent absorber can be obtained by tuning the change in the phase and amplitude of the electromagnetic wave as a result of Faraday rotation. A CPA using TWSs can be obtained by adjusting the appropriate polarizations given by the Faraday rotations together with exact phase and amplitude modulations [17–21]. This happens due to the fact that a CPA has the time reversal symmetry of a laser. With our study, it is possible to use the properties of TWSs as a tuning parameter in such applications.

In general, the nature of the nonlinear characteristics of materials is that the nonlinearity gives rise to a way to adjust the physical parameters and employ them for tuning purposes. Nonlinearity especially provides a powerful way to make adjustments to the system. In this way, the topological systems maintain their topologically robust features against perturbations in the relevant parameters. With regard to Weyl semimetals, the distance between Weyl nodes b can be used as an additional distinguished tuning parameter. This is the remarkable advantage of nonlinearities in such materials. Also, in this way, one can demonstrate how to find a range for the b parameter. This is a very active field on which intense studies are performed. Moreover, nonlinear optical responses are reproduced using a diagrammatic approach, which uses Feynman rules [22].

In Weyl semimetals, the unique electronic band structure near Weyl nodes leads to strong chiral optical responses, making them promising candidates for circular dichroism (CD)-based optical devices. If the orientation of the Weyl nodes is perpendicular to the polarization of the light, then the material will absorb less energy from the light. This is because the electric field of the light can interact less strongly with the Weyl nodes when they are not aligned. Therefore, the absorption of the material depends on the angle between the orientation of the Weyl nodes and the polarization of the light. This angle can be changed by rotating the material or the light source.

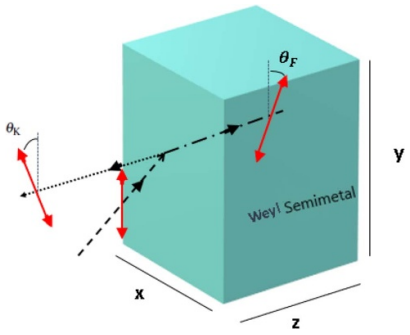

Figure 1. The interaction of a TE mode electromagnetic wave with a Weyl semimetal thin film. The incident wave is sent at an angle θ with the surface normal, and the polarization direction is rotated inside and outside the Weyl semimetal with angles θ_F and θ_K, respectively.

CD in Weyl semimetals can have potential applications in molecular spectroscopy and optical spectrometer technology. In molecular spectroscopy, by measuring the difference in absorption of left circularly polarized light and right circularly polarized light at different wavelengths, one can gain a CD spectrum, which can disclose facts about the shape and orientation of the molecules. Moreover, CD effects can be used to probe the topological nature of the Weyl semimetal and distinguish it from other types of materials, such as Dirac semimetals [23, 24]. In our study, we used the following pictorial demonstration in figure 1, which is originally designed as a one-dimensional transverse electric (TE) configuration, but Kerr and Faraday rotations turn the problem into a two-dimensional one.

In this study, the interaction of a nonlinear semimetallic topological material with an electromagnetic wave is investigated to reveal how the wave propagation is affected by a TWS. In section 2, brief information is given about the derivation of Maxwell equations for a TWS. In sections 3 and 4, one-dimensional linear and nonlinear Helmholtz equations are constructed for a TWS environment, respectively. The *tanh method* is successfully applied to find solutions of a nonlinear Helmholtz equation of light propagating in a TWS. In section 6, analytical solutions obtained by tanh and sech methods for a real case and numerical solutions for a complex case are presented. Finally, the conclusions of all our findings are provided in section 7.

2. Maxwell's equations for a TWS

The interaction of electromagnetic waves with TWSs is being investigated within the framework of a relatively new field of

physics, which is called topological photonics. The arrangement of Maxwell's equations in topological terms gives the nonlinear Helmholtz equation. The Helmholtz equation is a partial differential equation of the second order. It has many physical applications and is used in optics to describe electromagnetic waves propagating in a constant state. When boundary conditions are applied, the Helmholtz equation always produces a single solution. Before obtaining the nonlinear Helmholtz equation, the linear Helmholtz equation is derived. In this work only TE mode propagation is considered. Therefore, the electric field of an electromagnetic wave propagating in TE mode is parallel to the y-axis $\vec{E}//\vec{y}$, as seen in figure 2. TWS materials exhibit interesting physical behavior. One such example is the topological magneto-electric effect. The topological magneto-electric effect is a phenomenon when an electric field produces a magnetic field in the same direction (parallel to itself) as odd multiples of the fine structure constant, $\alpha = e^2/4\pi\varepsilon_0\hbar c$ [25]. Certain types of Weyl semimetals can exhibit strong CD, which can lead to a rotation of the polarization of an incident electromagnetic wave. The presence of the axionic term in a Weyl semimetal changes Maxwell's equation in the material. This axionic term has important implications for the polarization rotation of the reflected light. This axionic term also causes the topological magneto-electric effect. Since the axionic field in topological insulators is a constant, the axionic field in Weyl semimetal has a nontrivial dependence on space and time due to the breaking of time reversal and inversion symmetries. The axionic term is added to the Lagrangian density of the electromagnetic field with the following term $\delta\mathcal{L} = \beta\theta\mathbf{E}\cdot\mathbf{B}$. In the Maxwell equations, $\beta = 2\alpha/\pi Z_0$ is a constant, α is the fine structure constant, $Z_0 = \sqrt{\mu_0/\varepsilon_0}$ is the vacuum impedance, e is the charge of an electron and $c = 1/\sqrt{\varepsilon_0\mu_0}$ is the speed of light in vacuum. In a Weyl semimetal, $\theta(\mathbf{r},t) = 2\mathbf{b}\cdot\mathbf{r} - 2b_0 t$ is the expression of the axionic field. Here, b_0 and b are the distances between two Weyl nodes in the energy and momentum space, respectively. For a Weyl semimetal with inversion symmetry, we can set $b_0 = 0$. In materials that exhibit axion reactions, the electric displacement field and magnetic field may contain additional terms derived from the topological properties of the material. Magnetization, M and polarization, P can be derived from the Helmholtz free energy of the system, F. Therefore, the free energy must have the form, $F = \beta\theta\mathbf{E}\cdot\mathbf{B}$ [26, 27]. Maxwell equations including topological terms are written as

$$\begin{aligned} &\vec{\nabla}\cdot\overrightarrow{\mathcal{D}} = \rho(z) + \beta\vec{b}\cdot\overrightarrow{\mathcal{B}}, && \vec{\nabla}\cdot\overrightarrow{\mathcal{B}} = 0, \\ &\vec{\nabla}\times\overrightarrow{\mathcal{H}} - \partial_t\overrightarrow{\mathcal{D}} = \overrightarrow{\mathcal{J}}(z) - \beta\vec{b}\times\overrightarrow{\mathcal{E}}, && \partial_t\overrightarrow{\mathcal{B}} + \vec{\nabla}\times\overrightarrow{\mathcal{E}} = \overrightarrow{0}. \end{aligned} \tag{1}$$

Here, $\beta\vec{b}\cdot\vec{\mathcal{B}}$ and $-\beta\vec{b}\times\vec{\mathcal{E}}$ are called topological terms (see the appendix for the derivation of the topological terms). The vector notation $\vec{b}$ specifies the distance between two Weyl nodes, which are aligned in the z-direction, and is given explicitly by $\vec{b}(z) = b(z)\hat{e}_z$, and $b(z) = bH(z)H(L-z)$, where $H(z)$ is the Heaviside step function defined as

$$H(z) = \begin{cases} 0 & \text{for} \quad z < 0 \\ 1 & \text{for} \quad z > 0. \end{cases} \tag{2}$$

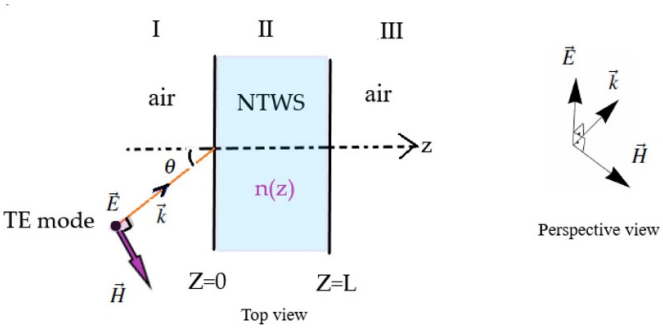

Figure 2. Sending an electromagnetic wave in TE mode with a wave vector $\vec{k}$ and incidence angle θ to the air–nonlinear TWS interface.

Under time dependent conditions, harmonic electric and magnetic fields are described as the following,

$$\vec{\mathcal{E}}(\vec{r},t) = \vec{E}(\vec{r})\,\mathrm{e}^{-\mathrm{i}\omega t}, \quad \vec{\mathcal{H}}(\vec{r},t) = \vec{\mathcal{H}}(\vec{r})\,\mathrm{e}^{-\mathrm{i}\omega t}. \tag{3}$$

By considering time harmonic electromagnetic waves, TE mode solutions can be regarded as obliquely incident in the form, see figure 1, where the E can be written as

$$\vec{E}(\vec{r}) = E(z)\,\mathrm{e}^{\mathrm{i}k_x x}\hat{e}_y \ . \tag{4}$$

Maxwell equations including topological terms at the free charge $\rho(z) = 0$ and free current density $j(z) = 0$ regions become,

$$\vec{\nabla}\cdot\vec{\mathcal{D}} = \beta\vec{b}\cdot\vec{\mathcal{B}}, \quad \vec{\nabla}\cdot\vec{\mathcal{B}} = 0, \tag{5}$$

$$\vec{\nabla}\times\vec{\mathcal{H}} = -i\omega\vec{\mathcal{D}} - \beta\vec{b}\times\vec{\mathcal{E}}, \quad \vec{\nabla}\times\vec{\mathcal{E}} = i\omega\vec{\mathcal{B}}. \tag{6}$$

Here, $\vec{\mathcal{E}}$ and $\vec{\mathcal{H}}$ are the electric and magnetic fields, as seen in figure 2. They are connected to $\vec{\mathcal{D}}$ and $\vec{\mathcal{B}}$ fields via the constitutive relations, $\vec{\mathcal{D}} = \tilde{\varepsilon}\vec{\mathcal{E}}$ and $\vec{\mathcal{B}} = \tilde{\mu}\vec{\mathcal{H}}$.

3. Linear Helmholtz equation for a TWS

In the case where the relative dielectric constant is not dependent on the electric field ($\tilde{\varepsilon} =$ constant; $\vec{b} =$ constant), the gradient of it can be taken as $\vec{\nabla}\tilde{\varepsilon} = 0$. When the dielectric coefficient is linear, the $\tilde{\mu}\tilde{\varepsilon}$ term can be taken as $\tilde{\mu}\tilde{\varepsilon} = \frac{1}{c^2}n^2$. Here, n is the complex refractive index of the TWS, and the relative dielectric constant is $\tilde{\varepsilon} = \varepsilon_0\varepsilon$. In this study, permeability is taken as $\tilde{\mu} = \mu_0$ since the material does not have magnetic properties. The Maxwell equations in (5) and (6) can be manipulated to give a three-dimensional Helmholtz equation associated with the TE mode states, and the corresponding magnetic field, $\vec{H}$, as follows

$$\nabla^2\vec{E} = -k^2n^2\vec{E} + ikZ_0\beta\vec{b}\times\vec{E}, \tag{7}$$

$$\vec{H} = -\frac{i}{kZ_0\mu(z)}\vec{\nabla}\times\vec{E}. \tag{8}$$

We stress that TE waves correspond to the solutions of equation (7), for which $\vec{\mathcal{E}}$ is parallel to the surface of the TWS.

In our geometrical setup, they are aligned along the y-axis, as seen in figure 2. Suppose that the incident wave $\vec{E}(\vec{r})$ adapts a plane wave with wave vector $\vec{k}$ in the x-z plane, specified by the following wave vector, $\vec{k} = k_x\hat{e}_x + k_z\hat{e}_z$, where $k_x = k\sin\theta$ and $k_z = k\cos\theta$. The TE mode solution of equation (7) in the view of Kerr and Faraday rotations can be established by means of the following one-dimensional coupled Helmholtz equations

$$E_x'' + \tilde{k}^2 E_x + ikZ_0\beta b E_y = 0 \tag{9}$$
$$E_y'' + \tilde{k}^2 E_y - ikZ_0\beta b E_x = 0 \tag{10}$$

where a prime denotes the derivative with respect to z. The piecewise constant function $\tilde{k}$ is specified by $\tilde{k} = k_z\tilde{n}$, where $\tilde{n} = \frac{\sqrt{n^2-\sin^2\theta}}{\cos\theta}$ and $\tilde{n}_\pm = \sqrt{\tilde{n}^2 \pm \frac{Z_0\beta b}{k\cos^2\theta}}$. Notice that refractive indices $\tilde{n}_\pm$ within the TWS slab lead to the birefringence effect.

3.1. Solutions to linear Helmholtz equation

The solutions of equations (9) and (10) are attained once we split them into uncoupled modes as follows,

$$\psi_\pm(z) = E_x(z) \pm iE_y(z) \tag{11}$$

where $\psi_\pm$ are the solutions of the following equations,

$$\psi_\pm'' + k_z^2 \tilde{n_\pm}^2 \psi_\pm = 0. \tag{12}$$

The solution to the above homogeneous linear differential equation (12) is given with $(+)$ and $(-)$ mode solutions as the following,

$$\psi_+ = A_1^+ e^{ik_z\tilde{n}_+ z} + A_2^- e^{-ik_z\tilde{n}_+ z} \tag{13}$$
$$\psi_- = B_1^+ e^{ik_z\tilde{n}_- z} + B_2^- e^{-ik_z\tilde{n}_- z}. \tag{14}$$

4. Nonlinear Helmholtz equation for a TWS

In the nonlinear case, the dielectric constant of a material becomes dependent on the electric field. The simplest nonlinear case is where the relative dielectric constant is directly proportional to the square of the electric field, $\tilde{\varepsilon} = \varepsilon_0(\varepsilon + \sigma|\vec{\mathcal{E}}|^2)$. Here, $\tilde{\varepsilon}$ is the permittivity of the TWS, which is a material with a nonlinear Kerr coefficient. Here, $\varepsilon = \varepsilon_b + \frac{i\sigma_{yy}}{\varepsilon_0\omega}$ is the frequency-dependent relative dielectric constant, including the bound charge contribution term ε_b and the σ_{yy} conductive term, σ is the Kerr coefficient and ε_0 is the permittivity of vacuum. Similarly, in the magnetic field perspective, $\tilde{\mu} = \mu_0\mu = 1 + \chi_m$ is the permeability of the related region, μ_0 is the permeability of vacuum; in our non-magnetic material case study, magnetic susceptibility χ_m is ignored. After arranging the Maxwell equations, the governing equation of the electromagnetic wave, which is called a one-dimensional nonlinear Helmholtz equation, can be obtained by the following steps. Taking ∇ of (6):

$$\nabla\times(\nabla\times E) = i\omega\left(-i\omega\mu_0\vec{D} - \mu_0\beta\vec{b}\times\vec{E}\right) \tag{15}$$

is obtained. From the equations in (5) the divergence of $\vec{E}$

$$\vec{\nabla}\cdot\vec{E} = \frac{\beta\vec{b}\cdot\vec{B} - \left(\vec{\nabla}\tilde{\varepsilon}\right)\vec{E}}{\tilde{\varepsilon}} \tag{16}$$

a is found. By using equation (15),

$$\begin{aligned}&\left[\beta\left(\vec{\nabla}\cdot\vec{b}\right)\cdot\vec{B} + \beta\vec{b}\cdot\left(\vec{\nabla}\cdot\vec{B}\right) - \vec{\nabla}\left(\vec{\nabla}\cdot\tilde{\varepsilon}\right)\vec{E} - \left(\vec{\nabla}\cdot\tilde{\varepsilon}\right)\left(\vec{\nabla}\cdot\vec{E}\right)\right]\tilde{\varepsilon}\\ &\quad - \left(\vec{\nabla}\cdot\tilde{\varepsilon}\right)\left\{\beta\vec{b}\cdot\vec{B} - (\nabla\tilde{\varepsilon})\vec{E}\right\} - \tilde{\varepsilon}^2\nabla^2\vec{E}\\ &= \tilde{\varepsilon}^2\mu_0\omega^2\tilde{\varepsilon}\vec{E} - i\tilde{\varepsilon}^2\omega\mu_0\beta\vec{b}\times\vec{E}\end{aligned} \tag{17}$$

by using equation (16)

$$\begin{aligned}&\nabla^2\vec{E} + \left[\mu_0\omega^2\tilde{\varepsilon} - \frac{2\left(\vec{\nabla}\tilde{\varepsilon}\right)^2}{\tilde{\varepsilon}^2} + \frac{\left[\vec{\nabla}\cdot\left(\vec{\nabla}\tilde{\varepsilon}\right)\right]}{\tilde{\varepsilon}}\right]\vec{E} - i\mu_0\omega\beta\vec{b}\times\vec{E}\\ &\quad - \frac{2i\beta}{\omega\tilde{\varepsilon}^2}\left(\vec{\nabla}\tilde{\varepsilon}\right)\vec{b}\cdot\left(\vec{\nabla}\times\vec{E}\right) = 0\end{aligned} \tag{18}$$
$$\nabla^2\vec{E} + \mathcal{A}(\tilde{\varepsilon})\vec{E} + \mathcal{B}(\tilde{\varepsilon})\left(\vec{b}\times\vec{E}\right) = 0 \tag{19}$$

is obtained, where the following substitutions are used

$$\mathcal{A}(\tilde{\varepsilon}) = \left[\mu_0\omega^2\tilde{\varepsilon} + \left[\frac{\tilde{\varepsilon}\left(\vec{\nabla}\left(\vec{\nabla}\tilde{\varepsilon}\right)\right) - 2(\nabla\tilde{\varepsilon})^2}{\tilde{\varepsilon}^2}\right]\right] \tag{20}$$
$$\mathcal{B}(\tilde{\varepsilon}) = \left[-\mu_0 w^2\tilde{\varepsilon}^2 + 2\left(\vec{\nabla}\tilde{\varepsilon}\right)\vec{\nabla}\right]\frac{i\beta}{w\tilde{\varepsilon}^2}. \tag{21}$$

When a propagating electromagnetic wave is selected along the z-direction due to Kerr and Faraday rotations, an electric field can have two components, as the following,

$$\vec{E} = E_x\hat{e}_x + E_y\hat{e}_y. \tag{22}$$

Each component of the $\vec{E}$ field, E_x and E_y, must satisfy equation (19) separately, as the following,

$$\nabla^2 E_x + \mathcal{A}(\tilde{\varepsilon})E_x - b\mathcal{B}(\tilde{\varepsilon})E_y = 0 \tag{23}$$
$$\nabla^2 E_y + \mathcal{A}(\tilde{\varepsilon})E_y + b\mathcal{B}(\tilde{\varepsilon})E_x = 0. \tag{24}$$

By defining a phasor like $\psi_\pm = E_x \pm iE_y$ and multiplying equation (24) with i, summing with equation (23) and multiplying equation (24) with i, and subtracting from equation (23), the following two equations can be obtained,

$$\nabla^2\psi_\pm + \mathcal{A}(\tilde{\varepsilon})\psi_\pm \pm ib\mathcal{B}(\tilde{\varepsilon})\psi_\pm = 0. \tag{25}$$

Thereafter, $\pm$ solutions are going to be called $(+)$ and $(-)$ mode solutions, respectively. Equation (25) can be made similar to the nonlinear Schrödinger equation,

$$-\nabla^2\psi + V\psi + \sigma|\psi|^2\psi = k^2\psi. \tag{26}$$

To accomplish this, the E_x and E_y components of the electric field

$$E_x(x,z) = E_x(z)e^{ik_x x} \text{ and } E_y(x,z) = E_y(z)e^{ik_x x} \tag{27}$$

are substituted into equations (23) and (24) and, after doing simple calculations:

$$\partial_z^2 E_x(z) + \left[\mathcal{A}(\tilde{\varepsilon}) - k_x^2\right] E_x(z) - b\mathcal{B}(\tilde{\varepsilon}) E_y(z) = 0 \quad (28)$$

$$\partial_z^2 E_y(z) + \left[\mathcal{A}(\tilde{\varepsilon}) - k_x^2\right] E_y(z) + b\mathcal{B}(\tilde{\varepsilon}) E_x(z) = 0 \quad (29)$$

is obtained, and again, using the phasor definition $\psi_\pm$ and multiplying equation (29) with i, summing with equation (28) and multiplying equation (29) with i, and subtracting from equation (28), the following two equations can be obtained.

$$\psi_\pm'' + \left[\mathcal{A}(\tilde{\varepsilon}) - k_x^2\right] \psi_\pm \pm ib\mathcal{B}(\tilde{\varepsilon}) \psi_\pm = 0 \quad (30)$$

where derivatives are taken with respect to z.

4.1. Simplification of the $\mathcal{A}(\tilde{\varepsilon})$ term

Using $\tilde{\varepsilon} = \varepsilon_0 \varepsilon$, $\tilde{\varepsilon} = n^2 + \sigma|\vec{E}|^2$, $\omega^2 = c^2 k^2$, $\tilde{n}_\pm = \sqrt{\tilde{n}^2 \pm \frac{2\alpha b}{\pi k \cos^2\theta}}$, $\tilde{n} = \frac{\sqrt{n^2 - \sin^2\theta}}{\cos\theta}$, $k_z^2 = k^2 \cos^2\theta$ relations and by inserting $\tilde{\varepsilon}$ and ϵ into equation (20), the $\mathcal{A}(\tilde{\varepsilon})$ term is simplified as the following,

$$\mathcal{A}(\tilde{\varepsilon}) = \mu_0 \varepsilon_0 \omega^2 \varepsilon + \frac{\varepsilon \varepsilon_0^2 \nabla(\nabla\varepsilon) - 2\varepsilon_0^2 (\nabla\varepsilon)^2}{\varepsilon^2 \varepsilon_0^2} \quad (31)$$

and by writing the $\mu_0 \varepsilon_0 = \frac{1}{c^2}, \frac{\omega^2}{c^2} = k^2$ terms into $\mathcal{A}(\tilde{\varepsilon})$, the following is obtained,

$$\mathcal{A}(\tilde{\varepsilon}) = \left[k^2 \varepsilon + \frac{\varepsilon \nabla(\nabla\varepsilon) - 2(\nabla\varepsilon)^2}{\varepsilon^2}\right] \quad (32)$$

by subtracting k_z^2 from both sides and using the definition of k_x and $\tilde{n}$, omitting σ^2 terms due to a small perturbation approximation and using

$$k_z^2 \tilde{n}^2 + \sigma k^2 |\vec{E}|^2 + \frac{\sigma n^2 \nabla\left(\nabla|\vec{E}|^2\right)}{n^4 + 2\sigma n^2 |\vec{E}|^2} = k_z^2 \tilde{n}^2 + \sigma k^2 |\vec{E}|^2 \frac{\sigma\left(\nabla\left(\nabla|\vec{E}|^2\right)\right)}{n^2 + 2\sigma|\vec{E}|^2} \quad (33)$$

$$\frac{1}{n^2 + 2\sigma\left(|\vec{E}|^2\right)} = \frac{n^2 - 2\sigma|\vec{E}|^2}{n^4}. \quad (34)$$

Equation $\mathcal{A}(\tilde{\varepsilon})$ becomes

$$\mathcal{A}(\tilde{\varepsilon}) - k_x^2 = k_z^2 \tilde{n}^2 + \sigma\left\{k|\vec{E}|^2 + \frac{\nabla\left(\nabla|\vec{E}|^2\right)}{n^2}\right\}. \quad (35)$$

4.2. Simplification of the $\mathcal{B}(\tilde{\varepsilon})$ term

By inserting $\tilde{\varepsilon} = \varepsilon_0 \varepsilon$ and $\varepsilon = n^2 + \sigma|\vec{E}|^2$ into equation (21) and setting the σ^2 term to zero, $\mathcal{B}(\tilde{\varepsilon})$ can be simplified to

$$\mathcal{B}(\tilde{\varepsilon}) = -i\beta\mu_0\omega + \frac{2i\beta\sigma}{\omega\varepsilon_0 n^4}\left(\nabla|\vec{E}|^2\right)\nabla. \quad (36)$$

4.3. Obtaining the nonlinear Helmholtz equation

By inserting equations (35) and (36) into equation (30) the nonlinear differential equation becomes

$$\psi_\pm'' + k_z^2 \tilde{n}^2 \psi_\pm \pm ib(-i\beta\mu_0\omega)\psi_\pm + \sigma\left\{\left[k^2|\vec{E}|^2 + \frac{\vec{\nabla}\cdot\left(\vec{\nabla}|\vec{E}|^2\right)}{n^2}\right] \pm ib\left(\frac{2i\beta}{\omega\varepsilon_0 n^4}\right)\left(\nabla|\vec{E}|^2\right)\cdot\vec{\nabla}\right\}\psi_\pm = 0 \quad (37)$$

where the following substitution is used for simplicity

$$\mathcal{C} = \left[k^2|\vec{E}|^2 + \frac{\vec{\nabla}\cdot\left(\vec{\nabla}|\vec{E}|^2\right)}{n^2}\right] \pm ib\left(\frac{2i\beta}{\omega\varepsilon_0 n^4}\right)\left(\nabla|\vec{E}|^2\right)\cdot\vec{\nabla}. \quad (38)$$

The term $\mathcal{C}$ is the source of nonlinearity, and after using shortening $\mathcal{C}$

$$\psi_\pm''(z) + \left(k_z^2\tilde{n}^2 \pm b\beta\mu_0\omega\right)\psi_\pm(z) + \sigma\mathcal{C}\psi_\pm(z) = 0 \quad (39)$$

is obtained. By using $c = \frac{1}{\sqrt{\varepsilon_0\mu_0}}, \beta = \frac{2\alpha}{\pi Z_0}, \omega = kc, Z_0 = \sqrt{\frac{\mu_0}{\varepsilon_0}}$ and $\beta\mu_0 w = \frac{2\alpha k}{\pi}$ terms

$$\psi_\pm'' + \left(k_z^2\tilde{n}^2 \pm \frac{2\alpha b k}{\pi}\right)\psi_\pm + \sigma\mathcal{C}\psi_\pm = 0 \quad (40)$$

by writing $\frac{2\alpha b k^2}{\pi k} \cdot \frac{\cos^2\theta}{\cos^2\theta}$ and using $k_z^2 = k^2\cos^2\theta$ then

$$\psi_\pm'' + k_z^2\left[\tilde{n}^2 \pm \frac{2\alpha b}{\pi k\cos^2\theta}\right]\psi_\pm + \sigma\mathcal{C}\psi_\pm = 0. \quad (41)$$

Afterward, by using $\tilde{n}_\pm^2 = \frac{n^2 \pm \sin^2\theta}{\cos^2\theta}$, the nonlinear Helmholtz equation for the TWS is obtained as the following

$$\psi_\pm'' + k_z^2\tilde{n}_\pm^2\psi_\pm + \sigma\mathcal{C}\psi_\pm = 0. \quad (42)$$

This equation is similar to the nonlinear Schrödinger equation,

$$-\psi_\pm'' - k_z(1 - \tilde{n}_\pm)\psi_\pm - \sigma\mathcal{C}\psi_\pm = k_z^2\psi_\pm \quad (43)$$

$$-\psi_\pm'' + V\psi_\pm - \sigma\mathcal{C}\psi_\pm = k_z^2\psi_\pm \quad (44)$$

where $V = k_z^2\left(1 - \tilde{n}_\pm^2\right)$ is the potential term and, if $k_z \in R$, the equation can be solved.

5. Solutions to the nonlinear Helmholtz equation

5.1. Real ψ case

If the $\psi_\pm$ function is assumed to be real, the electric field becomes simplified by writing $|\vec{E}|^2 = \psi_+^2 = \psi_-^2$. Equation (42) can be simplified to

$$\psi_{\pm}'' + k_z^2\tilde{n}_{\pm}^2\psi_{\pm} + \sigma k^2\psi_{\pm}^3 + \frac{2\sigma\left(\psi'_{\pm}\right)^2\psi_{\pm}}{n^2} + \frac{2\sigma}{n^2}\psi_{\pm}^2\psi_{\pm}'' \mp 2\sigma\left(\frac{2b\beta}{\omega\varepsilon_0 n^4}\right)\psi_{\pm}\left(\psi'_{\pm}\right)^2 = 0. \tag{45}$$

To simplify the above equation, the following substitutions are applied. Here, $a_{\pm} = k_z^2\tilde{n}_{\pm}^2$, $b = k^2\sigma$, $c_{\mp} = (\frac{2\sigma}{n^2} \mp \frac{2b\beta\sigma}{\omega\varepsilon_0 n^4}) = 2\sigma(\frac{1}{n^2} \mp \frac{2b\beta}{\omega\varepsilon_0 n^4})$ and $d = \frac{2\sigma}{n^2}$. Therefore, equation (45) becomes

$$\psi_{\pm}''\left(1 + d\psi_{\pm}^2\right) + \psi_{\pm}\left(a_{\pm} + b\psi_{\pm}^2 + c_{\mp}\left(\psi'_{\pm}\right)^2\right) = 0. \tag{46}$$

After replacing $\psi_{\pm}(z)$ with $u(z)$ for $(+/-)$ mode, the following equation is obtained

$$u''(z)\left(1 + du(z)^2\right) + u(z)\left(a_{\pm} + bu(z)^2 + c_{\mp}u'(z)^2\right) = 0. \tag{47}$$

To solve this nonlinear ordinary differential equation we have used the tanh method [6, 7]. When searching for tanh and sech type solutions to nonlinear differential equations, it is useful to apply $u(z) = \frac{1}{v(z)}$ transformation. Therefore, after substituting the first and second derivative of $u(z)$ as $u'(z) = -\frac{v'(z)}{v(z)^2}$ and $u''(z) = \frac{2v'(z)^2}{v(z)^3} - \frac{v''(z)}{v(z)^2}$ into equation (47), the nonlinear differential equation is converted as the following form,

$$\left(\frac{2v'(z)^2}{v(z)^3} - \frac{v''(z)}{v(z)^2}\right)\left(\frac{d}{v(z)^2} + 1\right) + \frac{a + \frac{b}{v(z)^2} + \frac{cv'(z)^2}{v(z)^4}}{v(z)} = 0. \tag{48}$$

Application of the tanh method gives four solutions to $v(t)$. After taking the inverse of the solutions, four $u(z)$ functions are obtained, as given below,

$$u_1(z) = \frac{\sqrt{b-ad}\sqrt{\frac{a^2d}{ad-b}}\coth\left(\phi - \frac{\sqrt{a}\sqrt{bz}}{\sqrt{2}\sqrt{b-ad}}\right)}{\sqrt{a}\sqrt{b}\sqrt{d}} \tag{49}$$

$$u_2(z) = \frac{a^{3/2}\sqrt{d}\coth\left(\phi - \frac{\sqrt{a}\sqrt{bz}}{\sqrt{2}\sqrt{b-ad}}\right)}{\sqrt{b}\sqrt{b-ad}\sqrt{\frac{a^2d}{ad-b}}} \tag{50}$$

$$u_3(z) = \frac{\sqrt{b-ad}\sqrt{\frac{a^2d}{ad-b}}\coth\left(\phi + \frac{\sqrt{a}\sqrt{bz}}{\sqrt{2}\sqrt{b-ad}}\right)}{\sqrt{a}\sqrt{b}\sqrt{d}} \tag{51}$$

$$u_4(z) = \frac{a^{3/2}\sqrt{d}\coth\left(\phi + \frac{\sqrt{a}\sqrt{bz}}{\sqrt{2}\sqrt{b-ad}}\right)}{\sqrt{b}\sqrt{b-ad}\sqrt{\frac{a^2d}{ad-b}}}. \tag{52}$$

Similarly, application of the sech method gives four solutions to $v(t)$. After taking the inverse of the solutions, four $u(z)$ functions are obtained, as given below,

$$u_1(z) = -\frac{\sqrt{-c-d}\sqrt{a - \frac{b}{c+d}}\cosh\left(\phi - \frac{\sqrt{b}z}{\sqrt{-c-d}}\right)}{\sqrt{b}\sqrt{c}} \tag{53}$$

$$u_2(z) = \frac{\sqrt{-c-d}\sqrt{a - \frac{b}{c+d}}\cosh\left(\phi - \frac{\sqrt{b}z}{\sqrt{-c-d}}\right)}{\sqrt{b}\sqrt{c}} \tag{54}$$

$$u_3(z) = -\frac{\sqrt{-c-d}\sqrt{a - \frac{b}{c+d}}\cosh\left(\phi + \frac{\sqrt{b}z}{\sqrt{-c-d}}\right)}{\sqrt{b}\sqrt{c}} \tag{55}$$

$$u_4(z) = \frac{\sqrt{-c-d}\sqrt{a - \frac{b}{c+d}}\cosh\left(\phi + \frac{\sqrt{b}z}{\sqrt{-c-d}}\right)}{\sqrt{b}\sqrt{c}}. \tag{56}$$

Afterward, we will label the $(+/-)$ mode coth-type (type 1) solutions with $\psi_{1i}^{\pm}$ and cosh-type (type 2) solutions with $\psi_{2i}^{\pm}$, where $i = 1, 2, 3, 4$. Therefore, in total we have 16 solutions, as follows: 4 $(+)$ mode coth , 4 $(-)$ mode coth, 4 $(+)$ mode cosh and 4 $(-)$ mode cosh-type solutions. These types of solutions are named solitons.

Within the context of mathematics and physics, when a soliton wave travels, its shape is preserved and its speed is also constant during its travel. This is interesting given the tendency of waves to disperse and dissipate. This is due to the balance between the nonlinearity and dispersion properties of the medium through which the wave travels. This property has practical applications in the fields of optical fibers and medical imaging [28].

Similarly, in the literature, Laine and Friberg [29] have shown four dark (tanh) and four bright (sech)-type solutions to nonlinear Schrödinger and nonlinear Helmholtz equations. The $(+/-)$ signs in the solutions are the topological charge of the soliton. Sometimes the $(+)$ and $(-)$ solutions are called kink and anti-kink solutions, respectively. At this point, after investigating our solutions, we can say that exact solutions of the nonlinear Helmholtz equation in a nonlinear Kerr medium reveal that the propagating wave is confined to its self-created waveguide. The same results are also obtained in the work of Laine and Friberg [29].

5.2. Complex ψ case

Here, we will consider E_x, E_x^* and E_y, E_y^* and construct ψ_+, ψ_- and their complex conjugates as the following:

$$\begin{aligned} \psi_+ &= E_x + i \quad E_y\psi_+^* = E_x^* - iE_y^*, \\ \psi_- &= E_x - i \quad E_y\psi_-^* = E_x^* + iE_y^*. \end{aligned} \tag{57}$$

After simple calculations $|\vec{E}|^2$ is found as

$$|\vec{E}|^2 = |E_x|^2 + |E_y|^2 = \frac{1}{2}\left(\psi_+\psi_+^* + \psi_-\psi_-^*\right). \tag{58}$$

After substituting $|\vec{E}|^2$ in to equations (42) and (38) we find:

$$\psi_{\pm}'' + k_z^2\tilde{n}_{\pm}^2\psi_{\pm} + \sigma\frac{k_z^2}{2\cos^2\theta}\left[\psi_+\psi_+^\star + \psi_-\psi_-^\star\right]\psi_{\pm} + \frac{\sigma}{2n^2}\frac{\mathrm{d}^2}{\mathrm{d}z^2}\left[\psi_+\psi_+^\star + \psi_-\psi_-^\star\right]\psi_{\pm} \mp \frac{b\beta\sigma}{\omega\varepsilon_0 n^4}\frac{\mathrm{d}}{\mathrm{d}z}\left[\psi_+\psi_+^\star + \psi_-\psi_-^\star\right]\psi'_{\pm} = 0 \tag{59}$$

where ψ_+ and ψ_- are forms coupled to ordinary differential equations for (E_x and E_y) as the following:

$$\begin{aligned}
&(E_x + iE_y)'' + k_z^2 \tilde{n}_+^2 (E_x + iE_y) \\
&+ \sigma \frac{k_z^2}{2\cos^2\theta} \left[2|E_x|^2 + 2|E_y|^2\right](E_x + iE_y) \\
&+ \frac{\sigma}{2n^2}\frac{\mathrm{d}^2}{\mathrm{d}z^2}\left(2|E_x|^2 + 2|E_y|^2\right)(E_x + iE_y) \\
&- \frac{b\beta\sigma}{\omega\varepsilon_0 n^4}\frac{\mathrm{d}}{\mathrm{d}z}\left(2|E_x|^2 + 2|E_y|^2\right)(E_x' + iE_y') = 0 \qquad (60) \\
&(E_x - iE_y)'' + k_z^2 \tilde{n}_-^2 (E_x - iE_y) \\
&+ \sigma \frac{k_z^2}{2\cos^2\theta} \left[2|E_x|^2 + 2|E_y|^2\right](E_x - iE_y) \\
&+ \frac{\sigma}{2n^2}\frac{\mathrm{d}^2}{\mathrm{d}z^2}\left(2|E_x|^2 + 2|E_y|^2\right)(E_x - iE_y) \\
&+ \frac{b\beta\sigma}{\omega\varepsilon_0 n^4}\frac{\mathrm{d}}{\mathrm{d}z}\left(2|E_x|^2 + 2|E_y|^2\right)(E_x' - iE_y') = 0 \qquad (61)
\end{aligned}$$

are obtained.

6. Results and discussion

As a model system, solutions of the nonlinear Helmholtz equation are investigated numerically for the Weyl semimetal TaAs. The physical parameters that are used in the calculations are listed in table 1. The (+) and (−) mode solutions do not differ significantly over the investigated z-range. This is because the numerical values of $\tilde{n}_+$, $\tilde{n}_-$ and parameter d in equation (47) do not significantly differ for (+) and (−) modes. Therefore, only (+) mode solutions are presented in this work.

6.1. Real ψ case

A snapshot of the wave specified by taking the phase value $\pi/4$ for coth and cosh-type solutions. Real and imaginary parts of the (+) mode coth-type solutions, $\mathrm{Re}(\psi_{1i}^+)$ and $\mathrm{Im}(\psi_{1i}^+)$, are given in figures 3(a) and (b). The $\mathrm{Re}(\psi_{11}^+)$ and $\mathrm{Re}(\psi_{14}^+)$, $\mathrm{Re}(\psi_{12}^+)$ and $\mathrm{Re}(\psi_{13}^+)$, $\mathrm{Im}(\psi_{11}^+)$ and $\mathrm{Im}(\psi_{13}^+)$, and $\mathrm{Im}(\psi_{12}^+)$ and $\mathrm{Im}(\psi_{14}^+)$ solutions are very close to each other over the investigated z-range. Real and imaginary parts of the (+) mode cosh-type solutions, $\mathrm{Re}(\psi_{2i}^+)$ and $\mathrm{Im}(\psi_{2i}^+)$, are given in figures 4(a) and (b). The $\mathrm{Re}(\psi_{21}^+)$ and $\mathrm{Re}(\psi_{24}^+)$, $\mathrm{Re}(\psi_{22}^+)$ and $\mathrm{Re}(\psi_{23}^+)$, $\mathrm{Im}(\psi_{21}^+)$ and $\mathrm{Im}(\psi_{23}^+)$, and $\mathrm{Im}(\psi_{22}^+)$ and $\mathrm{Im}(\psi_{24}^+)$ solutions are very close to each other over the investigated z-range.

Table 1. The values of the physical parameters that are used in this study with corresponding symbols.

Symbol	Explanation	Value
ϕ	Phase	$\frac{\pi}{4}$
θ	Incident angle	$\frac{\pi}{4}$
α	Fine structure constant	7.2974×10^{-3}
b	Distance between Weyl nodes (m)	7.85×10^{-9}
L	Thickness of the TWS (m)	1×10^{-6}
c	Speed of light $(\mathrm{m\,s^{-1}})$	299 792 458
ϵ_0	Permittivity of vacuum $(\mathrm{Fm^{-1}})$	8.85×10^{-12}
λ	Wavelength of incident light (m)	800×10^{-9}
μ_0	Permeability of vacuum $(\mathrm{NA^{-2}})$	1.25×10^{-6}
n	Refractive index of TaAs	6.3
σ	Kerr coefficient of TaAs $(\mathrm{m^2\,W^{-1}})$	1×10^{-8}
Z_0	Vacuum impedance (Ω)	376.73

As understood from figures 3 and 4, coth-type functions are inclined left or right, whereas cosh type solutions are more symmetric along the x-axis. The frequencies of the coth-type solutions are higher than those of the cosh-type solutions.

The norm of the (+) mode coth-type $|\psi_{1i}|^2$ and cosh-type $|\psi_{2i}|^2$ solutions is given in figure 5. These plots give some insight into the amplitude change in the investigated z-range. All the solutions in the $|\psi_{1i}|^2$ set and $|\psi_{2i}|^2$ set are very close to each over the investigated z-range.

For each type of solution, the real and imaginary parts of the ψ_{1i} and ψ_{2i} functions represent the electric field components E_x and E_y. In figures 6 and 7, the z-dependence of E_x and E_y is presented via a 3D parametric plot for coth- and cosh-type solutions, respectively. The coth-type ψ_{11} and ψ_{12} solutions present left circularly polarized light, whereas ψ_{13} and ψ_{14} solutions present right circularly polarized light. Meanwhile, cosh-type ψ_{21} and ψ_{22} solutions present right circularly polarized light, whereas ψ_{23} and ψ_{24} solutions present left circularly polarized light. Therefore, one can say that coth- and cosh-type solutions complement each other optically.

6.2. Complex ψ case

In the investigation of the complex ψ case, the coupled ordinary differential equations (60) and (61) are solved numerically. The initial conditions of E_x and E_y are selected in such a way so they form TE polarized incident light. When TE polarized light is incident on the TWS, it becomes right circularly polarized after passing through the material, as seen in figure 8.

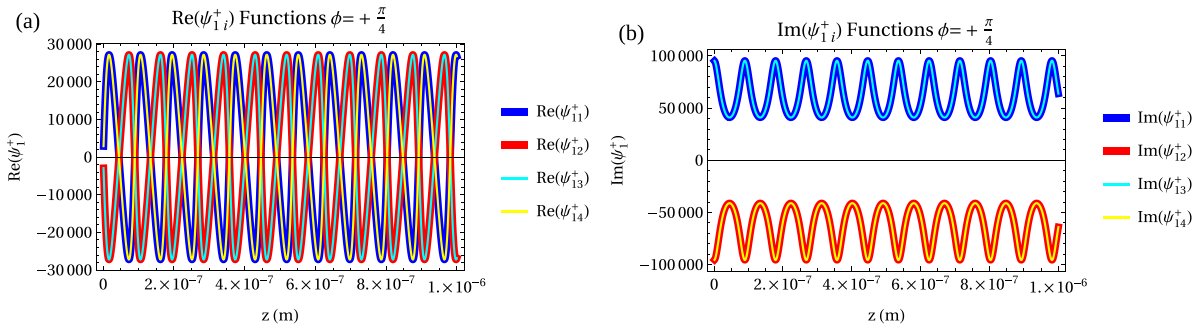

Figure 3. (a) Real and (b) imaginary parts of (+) mode coth-type solutions.

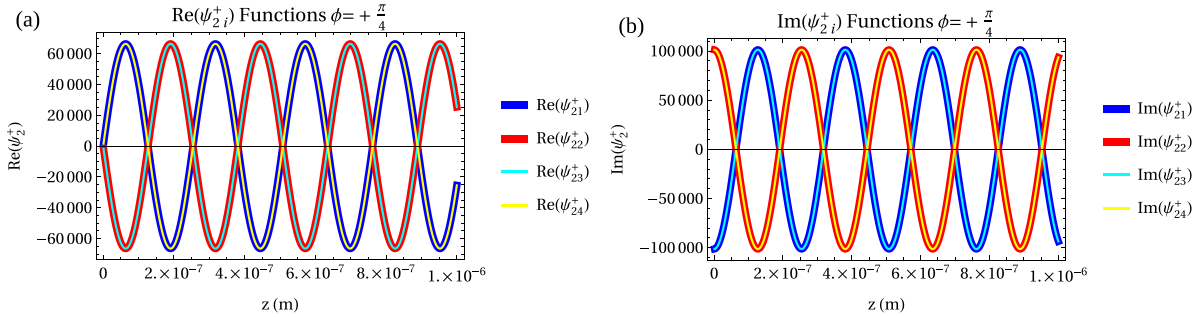

Figure 4. (a) Real and (b) imaginary parts of (+) mode cosh-type solutions.

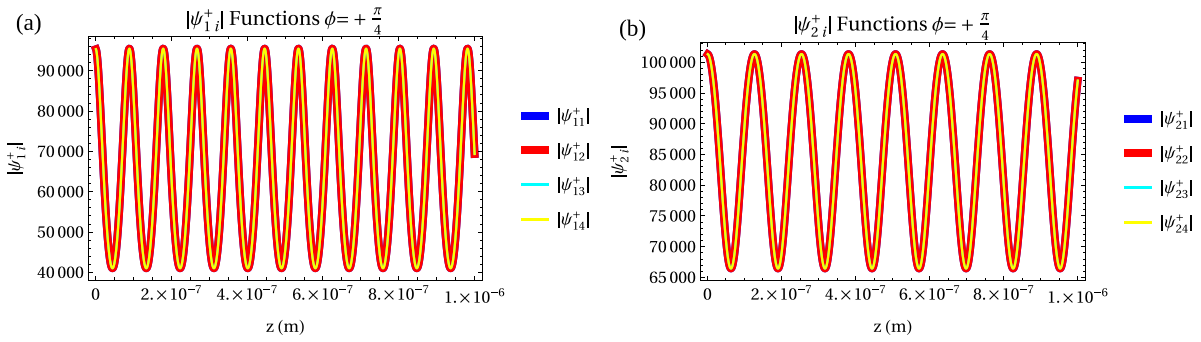

Figure 5. The norm square of (a) coth- and (b) cosh-type solutions.

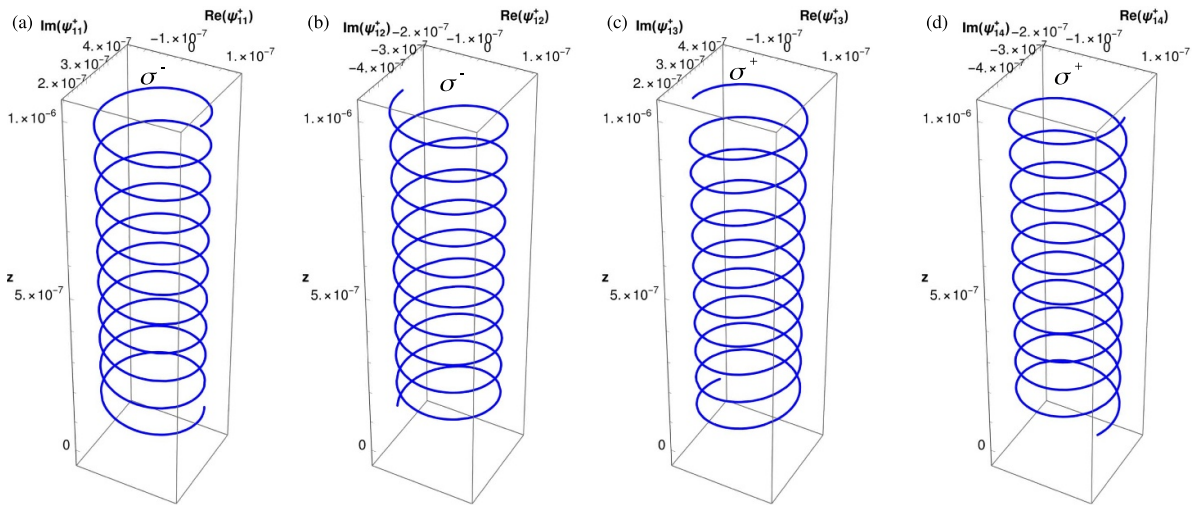

Figure 6. The electric field vector rotates counterclockwise (left circularly polarized light) (a), (b) and clockwise (right circularly polarized light) (c), (d) for the coth-type solutions.

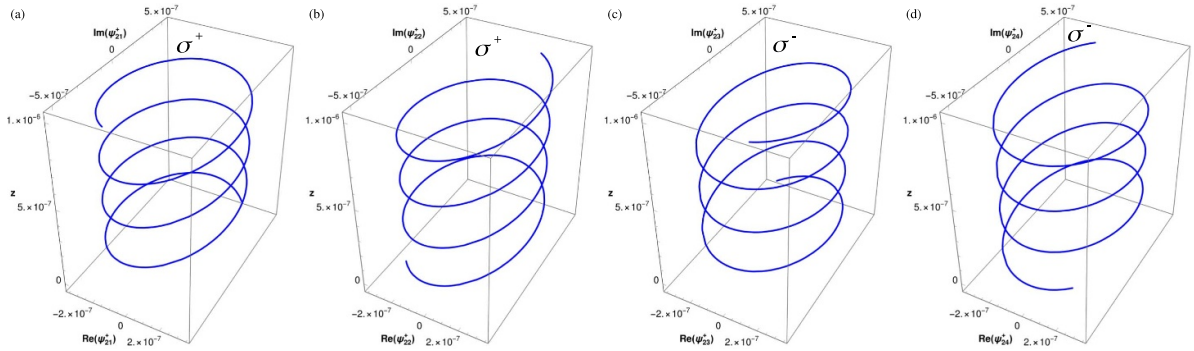

Figure 7. The electric field vector rotates clockwise (right circularly polarized light) (a), (b) and counterclockwise (left circularly polarized light) (c), (d) for the cosh-type solutions.

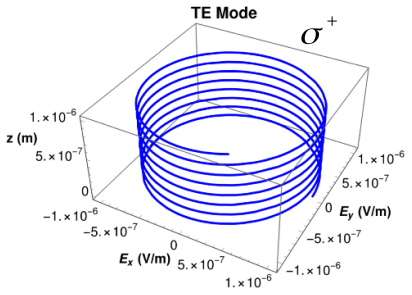

Figure 8. The electric field vector rotates clockwise (right circularly polarized light) for TE polarized incident light.

7. Conclusion

As a conclusion, two main (coth and cosh)-type and eight subtype solutions are found for TE mode light propagation in TWS material for the real ψ case with the help of the nonlinear Helmholtz equation, including topological terms. It is observed that for both coth- and cosh-type solutions, the electric field vector rotates counterclockwise (forms left circularly polarized light) in two types of solutions and clockwise (forms right circularly polarized light) in the other two types of solutions.

For the complex ψ case, the incident TE polarized light electric field vector rotates clockwise, and therefore becomes right circularly polarized light inside the TWS material. Therefore, in both cases, the solutions successfully show Kerr and Faraday rotations in a TWS material.

Studying TM mode configuration in view of nonlinear considerations would be quite intriguing since TM mode does not allow Kerr/Faraday rotations intrinsically. An induced current is present inside the bulk medium. This gives us a robust topological structure such that the system parameters' distance between the Weyl nodes b, angle of incidence of light θ and wavelength λ of it lead to topological quantization. However, the content of TM mode analysis is far beyond the aims and projections of the current study. We therefore restricted our attention to only TE mode solutions.

In the literature, the linear dichroism properties of TWS are investigated for the light which is incident on a surface bearing Fermi arcs [30]. In our work, light is sent to a surface of a TWS without Fermi arcs. Kerr and Faraday rotations with the nonlinear effects lead to distinct left and right circularly polarized light propagation in the TWS material. Moreover, if one assumes that both left and right circularly polarized light can propagate in the TWS at the same time, then the material can exhibit CD. The only requirement for CD behavior is the material's difference in absorption between the left and right circularly polarized light. Therefore, we can conclude that CD spectroscopy can also be used to investigate TWS materials, as referred to in the literature [23, 24].

Data availability statement

No new data were created or analyzed in this study.

Acknowledgment

M Sarisaman was supported by the Scientific Research Projects Coordination Unit (BAP) of Istanbul University Project Number FBA-2020-35018.

Appendix. Modified Maxwell equations in the presence of axions

$$D = \epsilon E + P \tag{A.1}$$
$$H = B/\mu - M. \tag{A.2}$$

Here, M and P are derived from Helmholtz free energy as $M = -\partial F/\partial B$ and $P = -\partial F/\partial E$

$$D = \epsilon E - \beta\theta B \tag{A.3}$$
$$H = B/\mu + \beta\theta E. \tag{A.4}$$

Here, ϵ is the dielectric tensor and μ is magnetic permeability. Maxwell's equations change due to these conditions as follows,

$$\nabla\cdot(\epsilon E - \beta\theta B) = \rho \Rightarrow \nabla\cdot(\epsilon E) = (\rho + \rho_\theta)\,. \tag{A.5}$$

Here, $\rho_\theta = \beta\nabla\theta\cdot B$ is the axionic charge density. From equation (A.4),

$$\nabla\times(B/\mu+\beta\theta\boldsymbol{E}) = J+\frac{\partial}{\partial t}(\epsilon E-\beta\theta B) \tag{A.6}$$

$$\nabla\times B = \mu J+\epsilon\mu\frac{\partial E}{\partial t}+J_\theta \tag{A.7}$$

are obtained. Here, $\boldsymbol{J}_\theta = -\beta\mu(\dot{\theta}\boldsymbol{B}+\nabla\theta\times\boldsymbol{E})$ is the current density due to the action field. For a Weyl semimetal with inversion symmetry, $b_0 = 0$; therefore, $\nabla\theta = b$ and $\dot{\theta} = 0$. Using $\vec{H} = \frac{\vec{B}}{\mu}$, equations (A.5) and (A.7) take the following forms,

$$\nabla\cdot\mathbf{D} = \rho+\beta\mathbf{b}\cdot\mathbf{B} \tag{A.8}$$

$$\nabla\times\mathbf{H} = \frac{\partial\mathbf{D}}{\partial t}+\mathbf{J}-\beta\mathbf{b}\times\mathbf{E}. \tag{A.9}$$

The other two Maxwell's equations remain unchanged as,

$$\nabla\cdot\mathbf{B} = 0 \tag{A.10}$$

$$\nabla\times\mathbf{E}+\partial_t\mathbf{B} = 0. \tag{A.11}$$

ORCID iDs

Helda Alomeare https://orcid.org/0000-0002-5796-8456
Ferhat Nutku https://orcid.org/0000-0002-2052-4894
Mustafa Sarısaman https://orcid.org/0000-0002-7148-0836

References

[1] Chen Q, Kutayiah A R, Oladyshkin I, Tokman M and Belyanin A 2019 Optical properties and electromagnetic modes of Weyl semimetals *Phys. Rev.* B **99** 075137
[2] Grassano D, Pulci O and Bechstedt F 2018 Validity of Weyl fermion picture for transition metals monopnictides TaAs, TaP, NbAs and NbP from *ab initio* studies *Sci. Rep.* **8** 3534
[3] Nematollahi F, Motlagh S A O, Apalkov V and Stockman M I 2019 Weyl semimetals in ultrafast laser fields *Phys. Rev.* B **99** 245409
[4] Nematollahi F, Motlagh S A O, Wu J, Apalkov V and Stockman M I 2019 Topological properties of Weyl semimetals in circularly-polarized ultrafast laser field (arXiv:1903.01657)
[5] Neubauer D 2017 Optical and magneto-optical investigations on 3D Dirac- and Weyl-semimetals *PhD Thesis* University of Stuttgart
[6] Malfliet W and Hereman W 1996 The tanh method: I. Exact solutions of nonlinear evolution and wave equations *Phys. Scr.* **54** 563–8
[7] Malfliet W and Hereman W 1996 The tanh method: II. Perturbation technique for conservative systems *Phys. Scr.* **54** 569–75
[8] Bandres M A, Wittek S, Harari G, Midya P, Ren J, Mordechai S, Christodoulides D N and Mercedeh K 2018 Topological insulator laser: experiments *Science* **359** eaar4005
[9] Harari G, Bandres M A, Lumer Y, Rechtsman M C, Chong Y, Mercedeh K, Christodoulides D N and Mordechai S 2018 Topological insulator laser: theory *Science* **359** eaar4003
[10] Mostafazadeh A 2009 Spectral singularities of a complex scattering potentials and infinite reflection and transmission coefficients at real energies *Phys. Rev. Lett.* **102** 220402
[11] Mostafazadeh A and Sarisaman M 2013 Spectral singularities and whispering gallery modes of a cylindrical gain medium *Phys. Rev.* A **87** 063834
[12] Mostafazadeh A and Sarisaman M 2013 Spectral singularities in the surface modes of a spherical gain medium *Phys. Rev.* A **88** 033810
[13] Naimark M A 1960 Investigation of the spectrum and the expansion in eigenfunctions of a non-selfadjoint differential operator of the second order on a semi-axis *Trudy Moscov. Mat. Obsc.* **3** 181 Russian 1954 English transl.: Amer Math. Soc. Transl. 2 16 103
[14] Guseinov G S 2009 On the concept of spectral singularities *Pramana J. Phys.* **73** 587
[15] Mostafazadeh A and Sarisaman M 2015 Lasing-threshold condition for oblique TE and TM modes, spectral singularities and coherent perfect absorption *Phys. Rev.* A **91** 043804
[16] Mostafazadeh A 2015 *Physics of Spectral Singularities Geometric Methods in Physics Trends in Mathematics* ed P Kielanowski, P Bieliavsky, A Odzijewicz, M Schlichenmaier and T Voronov (Springer) pp 145–65
[17] Mostafazadeh A and Sarisaman M 2012 Optical spectral singularities and coherent perfect absorption in a two-layer spherical medium *Proc. R. Soc.* A **468** 3224
[18] Mostafazadeh A and Sarisaman M 2016 Spectral singularities in the TE and TM modes of a $\mathcal{PT}$-symmetric slab system: optimal conditions for realizing a CPA-laser *Ann. Phys.* **375** 265–87
[19] Mostafazadeh A and Sarisaman M 2011 Spectral singularities of a complex spherical barrier potential and their optical realization *Phys. Lett.* A **375** 3387
[20] Sarisaman M and Tas M 2019 Broadband coherent perfect absorber with $\mathcal{PT}$-symmetric 2D-materials *Ann. Phys.* **401** 139–48
[21] Sarisaman M and Tas M 2018 $\mathcal{PT}$-symmetric coherent perfect absorber with graphene *J. Opt. Soc. Am.* B **35** 2423
[22] Parker D E, Morimoto T, Orenstein J and Moore J E 2019 Diagrammatic approach to nonlinear optical response with application to Weyl semimetals *Phys. Rev.* B **99** 045121
[23] Hosur P and Qi X L 2015 Tunable circular dichroism due to the chiral anomaly in Weyl semimetals *Phys. Rev. B* **91** 081106
[24] Yu R, Weng H, Fang Z, Ding H and Dai X 2016 Determining the chirality of Weyl fermions from circular dichroism spectra in time-dependent angle-resolved photoemission *Phys. Rev.* B **93** 205133
[25] Oktay G, Sarisaman M and Tas M 2020 Lasing with topological Weyl semimetal *Sci. Rep.* **10** 3127
[26] Sonowal K, Singh A and Agarwal A 2019 Giant optical activity and Kerr effect in type-I and type-II Weyl semimetals *Phys. Rev.* B **100** 085436
[27] Sekine A and Nomura K 2021 Axion electrodynamics in topological materials *J. Appl. Phys.* **129** 141101
[28] Mollenauer L F and Gordon J P 2006 *Solitons in Optical Fibers* pp 195–229
[29] Laine T A and Friberg A T 2000 Self-guided waves and exact solutions of the nonlinear Helmholtz equation *J. Opt. Am.* B **17** 751
[30] Kargarian M, Randeria M and Trivedi N 2015 Theory of Kerr and Faraday rotations and linear dichroism in topological Weyl Semimetals *Sci. Rep.* **5** 1